

## Simulations of Sunyaev-Zel'dovich maps and their applications

J. Delabrouille<sup>1</sup>, J.-B. Melin<sup>1</sup> and J.G. Bartlett<sup>1,2</sup>

1. PCC - Collège de France, 11, place Marcelin Berthelot, 75231 Paris cedex 05

2. Physics Department, Université Paris 7-Denis Diderot

**Abstract.** We describe a fast method to simulate in a semi-analytical way consistent maps of the thermal, kinetic and polarised Sunyaev-Zel'dovich effect, featuring both cluster spatial correlations and large-scale velocity flows.

### 1. Introduction

There are a large number of applications for simulated maps of the Sunyaev-Zel'dovich (SZ) emission of galaxy clusters. Such maps are being used, for instance, to assess the capabilities of instruments dedicated to the SZ observations, or for the development of data analysis tools. They can also be used to constrain models of structure formation and/or cosmological parameter sets by comparison to real data.

There already exists a large number of tools to simulate SZ maps (Bond et al. 1996, Aghanim et al. 1997, da Silva et al. 2000, Kay et al. 2001, Kneissl et al. 2001, da Silva et al. 2001). Such tools range from simple uncorrelated Poisson distributions of idealised clusters to sophisticated hydro-codes simulating the complex physical process of structure formation, including non-linear gravity and some additional ingredients, such as magnetic fields, dissipation... While the former may be over simplistic for a range of applications, the latter require large computing facilities and extensive computer time, and do not illuminate simply the influence of the code inputs on the final results. In the approach presented here, we develop a code for simulating SZ maps that is fast enough to permit numerous Monte-Carlo simulations in a wide range of cosmological scenarios, while being accurate enough to correctly account for all three SZ effects (thermal, kinetic and polarised) and their distribution in both real and velocity space (e.g., bulk flows) according to the underlying spectrum of density fluctuations  $P(k)$ .

### 2. The SZ effect and galaxy clusters

Observations of galaxy clusters are useful as a probe of cosmology, and observations of the SZ effect in particular present various advantages in this light. Most notably, as galaxy clusters are the largest bound objects in our Universe, their distribution as a function of redshift is extremely sensitive to the history of

large-scale structure formation. With its distance independence, the SZ effect is ideal for tracing this history out to large redshifts, and thereby for providing stringent constraints on models. The SZ effect, although for long below attainable instrumental sensitivity, now represents an established and unbiased tool for the detection of distant clusters and for the estimation of their hot gas content. In particular, the Planck mission, to be launched by ESA in 2007, will produce an all-sky catalog of several tens of thousands of clusters, which will be used to constrain scenarios of structure formation and cosmological parameters, for example, through cluster count tests. In addition, SZ-selected cluster catalogs will be useful to constrain the two-point correlation function of clusters, and hence the matter power spectrum  $P(k)$  on the largest scales.

The kinetic and polarized SZ effect, although much more difficult to detect than the thermal SZ, also appear as extremely promising tools, allowing the determination of both radial and transverse velocities for clusters. Although detecting the polarised SZ effect still appears only marginally possible (Audit & Simmons 1999, Sazonov & Sunyaev 1999), the measurement of bulk radial velocities through the kinetic SZ effect seems within the reach of upcoming instruments (Aghanim et al. 1997). Both will become of ever greater importance for cosmology as instruments improve.

### **2.1. Why a new code for simulating SZ effect maps**

A key issue in interpreting SZ observations is the understanding of the selection function for clusters and of the importance of measurement errors. The assessment both requires testing methods for the extraction of the relevant SZ observables on simulated observations that accurately model the cluster population – gas physics and distribution in both real and velocity space – as well as instrumental effects and relevant astrophysical foregrounds. The simulations should be performed over a wide range of cosmological scenarios. As an example, one expects that in the near future direct constraints of cosmological parameters will be obtained from SZ cluster counts and redshift distributions. Likelihood contours may be obtained using analytical predictions of cluster counts (or cluster distributions in the observable parameter space), but the approach must be tested using Monte-Carlo simulations with numerous realisations of the observations and subsequent data analysis. Clearly, this can not be done using full-scale structure formation codes simulating gravitational collapse, as such codes require days or weeks of computation on supercomputers.

Our goal is to simulate maps accurate enough that they reliably feature the physical properties that convey cosmological information (e.g., cluster counts, cluster correlations in real space, bulk flows), in computation times permitting one to test methods statistically on thousands of simulations over a wide range of cosmologies.

### **2.2. The formation of cluster sized dark-matter haloes**

The formation of large haloes takes place through the gravitational instability of dark matter density fluctuations. Original density fluctuations (at the time of matter radiation decoupling), still well within the linear regime, grow through gravitational instability into the non-linear regime (when the density contrast  $\delta = \delta\rho/\rho$  becomes of order unity). Collapsed haloes of dark matter appear

where gravitational attraction overcomes the expansion and the density contrast becomes larger than some limit. The Press-Schechter (PS) formalism (1974) predicts the average number of such dark haloes as a function of mass,  $M$ , and redshift,  $z$ , for Gaussian fluctuations:

$$\frac{dN}{d \ln M dV_c} = \sqrt{\frac{2}{\pi}} \frac{\rho_0}{M} \nu \left| \frac{d \ln \sigma(0, M)}{d \ln M} \right| \exp(-\nu^2/2) \quad (1)$$

where  $\nu = \delta_c(z)/\sigma(z, M)$ ,  $\rho_0$  is the present average matter density,  $dV_c$  the covolume element,  $\delta_c(z) \simeq 1.68$  the critical density contrast necessary for the collapse, and  $\sigma(z, M) = D_g(z)\sigma(0, M)$  is the linear density fluctuation amplitude evolving according to the linear growth factor  $D_g(z)$  ( $\equiv 1$  at  $z = 0$ ). The fluctuation amplitude  $\sigma(z, M)$  is related to the power spectrum  $P(k)$  by:

$$\sigma^2(z, M) = D_g^2(z) \frac{1}{2\pi^2} \int_0^\infty k^2 P(k) W(k)^2 dk \quad (2)$$

where  $W(k)$  is the Fourier transform of a 3D tophat smoothing window function of size  $R = (3M/4\pi\rho)^{1/3}$ . The power spectrum  $P(k)$ , however, enters this formalism only through its integral value (the variance of the fluctuations); therefore, the formalism cannot account for the spatial correlation of clusters. Simulations based simply on PS result in maps that can only reproduce the predicted number of collapsed halos as a function of redshift, and not the cluster two-point correlation compatible with the underlying  $P(k)$ .

The power spectrum uniquely defines the two-point correlation properties of the density perturbation field,  $\delta$ . Kaiser (1984) was the first to suggest that clusters trace the density field in a biased fashion, preferentially forming in overdense regions:

$$N_{\text{clusters}} \propto 1 + b\delta \quad (3)$$

where the bias parameter  $b(M, z)$  is in general a function of both mass and redshift. This behavior is explained by the fact that galaxy clusters form from only the rarest, highest density peaks in the density field, and it is borne out by large N-body simulations; for example, Sheth et al. (2001) give an analytic expression for  $b(M, z)$ , based on earlier work of Mo & White (1996), that matches the clustering seen in simulations. We note in passing that, also from studies of clustering in large N-body simulations, the Press-Schechter formula is known to somewhat over-predict the number density of small mass dark haloes and to underestimate large haloes. These studies have lead to improved expressions for halo number density (e.g., Jenkins et al. 2001).

### 2.3. Cluster velocities

Cluster velocities are needed for the simulation of both kinetic SZ (radial part) and polarised SZ maps (transverse part). In the simplest simulation approach, the velocity of each individual cluster can be drawn at random from a 3D Gaussian probability distribution with *rms* proportional to the square root of the integrated velocity power spectrum:

$$\sigma_v(z, M) = a(z)H(z)f(\Omega_m, \Lambda) \left[ \frac{1}{8\pi^3} \int_0^\infty 4\pi D_g^2(z) P(k) W(k)^2 dk \right]^{1/2} \quad (4)$$

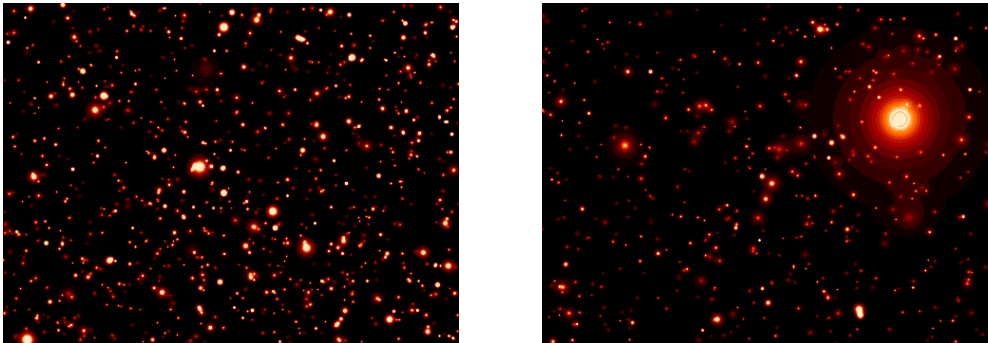


Figure 1. Thermal SZ map of 3 by 4 square degrees for a universe with  $\Omega_m = 0.3$ ,  $\Lambda = 0.7$ ,  $h = 0.65$ ,  $\Omega_b = 0.05$  (left panel), and with  $\Omega_m = 1$ ,  $\Lambda = 0$ ,  $h = 0.5$ ,  $\Omega_b = 0.07$  (right panel). Note that because of the different baryon fraction, the  $\Lambda$  universe clusters are brighter in SZ (respective color scales have been chosen such that they range from  $y = 0$  to  $y = 4 \times 10^{-5}$  on the left panel, and from  $y = 0$  to  $y = 1.5 \times 10^{-5}$  on the right one, with higher values saturated).

with  $a(z) = 1/(1+z)$  and  $H(z) = H_0 \sqrt{\Omega_m(1+z)^3 + (1 - \Omega_m - \Lambda)(1+z)^2 + \Lambda}$ . The function  $f$  is defined as  $f \equiv d \ln D_g(z) / d \ln a$ . Such an approach results in velocities which have the proper magnitude, but which are not correlated from one cluster to the next (i.e., no bulk flows). For sensitivity reasons, and because of confusion due to the primordial CMB fluctuations (and other foregrounds), upcoming experiments will not be able to measure individual cluster velocities (Haehnelt and Tegmark 1996, Aghanim et al. 2001). An estimate of the ability of instruments like Planck to measure peculiar velocities on large scales can be obtained by extrapolating the expected accuracy on a single cluster to a larger number of clusters moving together in a bulk flow (Aghanim et al. 2001). However, a more accurate study of this approach and its uncertainties requires simulations that correctly model large-scale velocity correlations. We detail such a method in the next section.

### 3. Simulation method

#### 3.1. The cluster spatial distribution

Since the power spectrum of density fluctuations,  $P(k)$ , uniquely defines the density field responsible for the formation of halos and their clustering, we start with a random realisation of the density contrast in a 3D comoving box, with the user placed at one end. The size of the box is matched to the size of the required map (angular extent). For a 3 degree-by-3 degree map, typical comoving box sizes (extending to a redshift of 5) are  $600 \times 600 \times 6000$  Mpc, divided in resolution cells of about 20 Mpc. To account for the different redshifts seen by the observer while looking through the box, the density field is scaled by the linear growth factor,  $D_g(z)$ , over slices of redshift (distance from the user). A random catalog

within the box is first constructed by drawing from a Poisson distribution with average given by the PS law (or Sheth-Tormen, or Jenkins et al., as appropriate, up to the user of the simulation tool) the number of clusters in a grid of mass bins for each redshift shell. The average can be slightly modified to take into account the fact that the particular redshift shell might be slightly overdense or underdense with respect to the ensemble average. For each shell, we then distribute the clusters in  $(\theta, \phi)$  with a probability proportional to  $1 + b\delta$ , where  $\delta$  is the density field scaled to the redshift of the shell and  $b$  the clustering bias. In this way, we construct a cluster distribution compatible with the underlying  $P(k)$  (within the resolution of the code).

### 3.2. Cluster peculiar velocities

The peculiar velocity of each cluster is found using linear theory applied to the density field realisation,  $\delta\rho/\rho$ . With the assumption that the peculiar velocity field is irrotational, as expected in most scenarios of structure formation, the velocity field can then be obtained from the Newtonian gravitational potential through

$$v = -\frac{2}{3} \frac{f(z)}{\Omega_m(z)H(z)} \frac{\nabla\Phi}{a} \quad (5)$$

where the gravitational potential  $\Phi$  is connected to  $\delta = \delta\rho/\rho$  by

$$\nabla^2\Phi = 4\pi G a^2 \delta\rho \quad (6)$$

### 3.3. Cluster gas properties

The physical modeling of individual clusters is a complicated issue, in principle calling into play a variety of physical processes. As spectacularly illustrated by the new X-ray satellites XMM-Newton and Chandra, clusters are not simple objects, but rather display complex substructures and inhomogeneities. For large maps which will be observed at low angular resolution (as will be the case for the Planck mission, for instance), these substructures are lost and thus not very important for the final properties of the map. For resolved clusters, on the other hand, proper physical modeling of cluster substructure is an important issue.

In our current simulations, we adopt a simple, self-similar cluster model based on an isothermal  $\beta$  model:

$$n_e(r) = n_e(0) \left( 1 + \left( \frac{r}{r_c} \right)^2 \right)^{-3\beta/2} \quad (7)$$

for the density profile, and a gas temperature-mass relation normalized to numerical simulations (Evrard et al. 1996):

$$T_e = 6.8h^{2/3} \left( \frac{M}{10^{15}M_\odot} \right)^{2/3} \left( \frac{\Omega_m \Delta_{NL}(z)}{178} \right)^{1/3} (1+z) \text{ keV} \quad (8)$$

where  $\Delta_{NL}(z)$  is the non-linear density contrast on collapse (a weak function of both  $\Omega$  and  $\Lambda$  that equals 178 in a critical universe). The virial radius is given

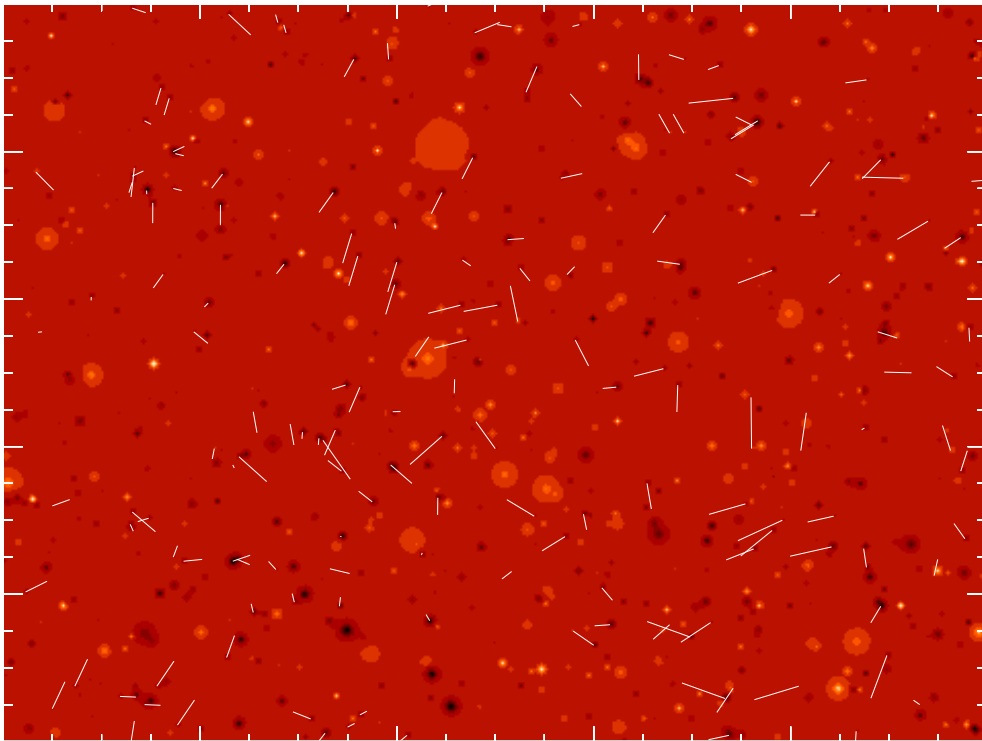


Figure 2. Velocity map of 3 by 4 square degrees.

by (e.g., Bartlett 1997)

$$r_v = 1.69h^{-2/3} \left( \frac{M}{10^{15}M_\odot} \right)^{1/3} (1+z)^{-1} \left( \frac{178}{\Omega_m \Delta_{NL}(z)} \right)^{1/3} \text{ Mpc} \quad (9)$$

Another possible approach is to replace this simple cluster model by maps of the Comptonization parameter  $y$  and/or the optical depth  $\tau$  obtained in detailed simulations of individual clusters, as done by Kneissl et al. (2001).

#### 4. Examples of maps obtained with the software

In Figure 1 we show  $3 \times 4$  degree<sup>2</sup> SZ maps simulated with our code for two different cosmologies, one with ( $\Omega_m = 0.3$ ,  $\Lambda = 0.7$ ,  $h = 0.65$ ,  $\Omega_b = 0.05$ ), left panel, and one with ( $\Omega_m = 1$ ,  $\Lambda = 0$ ,  $h = 0.5$ ,  $\Omega_b = 0.07$ ), right panel. The visual difference between the two maps is striking, with more high redshift clusters in the  $\Lambda$ -model than in the critical model (Barbosa et al. 1996).

As another example, we show in Figure 2 a peculiar velocity map where radial velocities are coded in color (the map is one of radial velocity times optical depth,  $\beta_r \tau$ ). Transverse velocities for clusters between redshifts 0.8 and 1 are indicated by the small arrows starting from the center of each cluster. The tangential velocities in this limited redshift slice demonstrate clear correlations on large scales. Maps of the polarised emission are straightforwardly obtained from the optical depths and transverse velocities, but are not shown here due to a lack of space.

#### 5. Characteristics of the code

The software can produce simulations for critical, open or closed CDM-like models, with or without a cosmological constant. A future development will be the inclusion of an arbitrary equation-of-state for the dark energy term (Quintessence). Presently, our software can only produce small tangential maps of limited fractions of the sky, although we are currently working on full-sky extensions. The software is implemented in the IDL programming language, and requires only a couple minutes on a modest PC to produce a map of several degrees squared.

#### 6. Conclusion

We have written a fast code for the simulation of SZ maps (thermal, kinetic and polarised) based on a simple model of cluster physics and on Monte Carlo realizations of the mass function and the linear density field. The code produces a cluster distribution and large-scale peculiar velocities consistent with the underlying power spectrum,  $P(k)$ . The software can produce maps for any kind of open, closed or critical universe, with or without a cosmological constant. With the expectation of data from the new generation of SZ dedicated instruments, this will be a useful tool for a wide range of applications, from optimizing observations strategies and devising/testing data processing methods, to constraining cosmological scenarios with real data.

**7. References****References**

- N. Aghanim et al. 1997, 325, 9
- N. Aghanim, K.M. Górski & J.-L. Puget 2001, *A&A* 374, 1
- E. Audit & J.F.L. Simmons 1999, *MNRAS* 305, 27
- D. Barbosa, J.G. Bartlett, A. Blanchard & J. Oukbir 1996, *A&A* 314, 13
- J.G. Bartlett 1997, in : *From Quantum Fluctuations to Cosmological Structures*, eds. D. Valls-Gabaud, M.A. Hendry, P. Molaro et al., *ASP Conf. Series* 126, 365
- J.R. Bond & S.T. Myers 1996, *ApJ Suppl. Ser.*, 103, 63
- A.C. da Silva, D. Barbosa, A.R. Liddle, P.A. Thomas 2000, *MNRAS* 317, 37
- A.C. da Silva, D. Barbosa, A.R. Liddle, P.A. Thomas 2001, *MNRAS* 326, 155
- A.E. Evrard, C.A. Metzler & J.F. Navarro 1996, *ApJ* 469, 494
- M.G. Haehnelt & M. Tegmark 1996, *MNRAS* 279, 545
- A. Jenkins et al. 2001, *MNRAS* 321, 372
- N. Kaiser 1984, *ApJ* 284, L9
- S.T. Kay, A.R. Liddle & P.A. Thomas 2001, *MNRAS* 325, 835
- R. Kneissl et al., 2001, submitted to *MNRAS* (astro-ph/0103042)
- H.J. Mo & S.D.M. White 1996, *MNRAS* 282, 347
- W.H. Press & P. Schechter 1974, *ApJ* 187, 425
- S.Y. Sazonov & R.A. Sunyaev 1999, *MNRAS* 310, 765
- R.K. Sheth, H.J. Mo & G. Tormen 2001, *MNRAS* 323, 1